ARTICLE

Elastic Properties and Morphology of Individual Carbon Nanofibers

Joseph G. Lawrence,[†] Lesley M. Berhan,[‡] and Arunan Nadarajah[†,*]

[†]Department of Chemical & Environmental Engineering and [‡]Department of Mechanical, Industrial & Manufacturing Engineering, University of Toledo, Toledo, Ohio 43606

ABSTRACT The structural complexity of vapor-grown carbon nanofibers means that they require a method that determines both their elastic properties and their corresponding morphology. A three-point bending test method was developed combining atomic force microscopy, transmission electron microscopy (TEM) and focused ion beam techniques to suspend individual nanofibers and measure their deflection coupled with accurate determinations of inner and outer diameters and morphology using high resolution TEM. This resulted in much improved accuracy and reproducibility of the measured values of the elastic modulus which ranged from 6 to 207 GPa. The data showed two distinct trends, with higher values of the modulus when the outer wall thickness of the nanofibers is larger than that of the inner wall, with the values decreasing with the overall wall thickness. These results suggest that the more ordered layers of the outer wall, closest to the inner wall, are mostly responsible for the nanofiber strength. For large nanofiber wall thicknesses of greater than 80 nm, the elastic modulus becomes independent of the thickness with a value of ~25 GPa. The results also demonstrate that this technique can be a standardized one for the detailed study of mechanical properties of nanofibers and their relationship to morphology.

KEYWORDS: carbon nanofibers · elastic modulus · morphology · cone angle · transmission electron microscopy

Vapor-grown carbon nanofibers (VGCNFs) lack the structural perfection of single wall carbon nanotubes (SWCNTs), but are believed to have similar thermal and mechanical properties. Unlike SWCNTs, VGCNFs are synthesized in a continuous reactor with floating catalysts employing a variety of hydrocarbon sources.[1,2] As a result, they can be produced commercially in large quantities at a much lower cost.[3] This combination of excellent multifunctional properties, commercial availability, and low cost has led to great interest in their use in a variety of applications, such as for fillers in polymer nanocomposites.[3–6] However, their widespread use has been hampered by the lack of a definitive understanding of their structure and properties.

VGCNFs have a unique hybrid graphene sheet structure based on both conical and tubular elements, unlike the solely tubular structure of carbon nanotubes. Additionally, heat-treated carbon nanofibers undergo a structural transformation, characterized by graphitization. This relative complexity has led to some confusion in earlier studies about the structure of these materials.[7,8] However, recent theoretical and structural studies have led to a more precise understanding of their structure, with two types of nanofibers present. The more abundant conical nanofibers have an inner layer composed of a perfect cone-helix structure and an outer layer composed of an imperfect or disordered multiwall nanotube-like structure.[9,10] The much less abundant bamboo nanofibers have a segmented structure that is more closely related to nanotubes. When heat treated the conical nanofibers undergo a transformation where the outer layer acquires a perfect multiwall nanotube structure and the inner layer acquires a segmented stacked cone structure.

The structural complexity of carbon nanofibers poses considerable difficulties in determining their elastic properties. This is in contrast to nanotubes, particularly SWCNTs, whose relative structural simplicity allows them to be characterized more directly. Additionally, the greater structural perfection of carbon nanotubes allows them to approach the high theoretical maximum strength of carbon−carbon bonds in graphite. While measuring the strength of any nanomaterial is a difficult undertaking, in recent years direct measurement methods have been developed primarily based on (a) bending tests with atomic force microscopes (AFM),[11–14] (b) vibration measurements with TEM,[15,16] or (c) direct tensile measurements with AFM and SEM.[17–19] These have largely confirmed that

*Address correspondence to nadarajah@utoledo.edu.

Received for review December 21, 2007 and accepted April 28, 2008.

Published online May 10, 2008.
10.1021/nn7004427 CCC: $40.75

SWCNTs and MWCNTs have elastic moduli and tensile strengths close to the theoretical maxima of ~1 TPa and ~150 GPa, respectively.

The lack of structural perfection and the existence of a complex hybrid structure mean that the strength of VGCNFs does not depend solely on graphitic carbon−carbon bonds. It follows that it is almost impossible to obtain theoretical predictions for their strength without extensive simplifications and assumptions.[20] It also precludes the use of some techniques such as vibration measurements. AFM-based bending tests are perhaps the only approach and some attempts have been made to measure the elastic moduli of nanofibers in this manner,[13,14] but reliable measurements have been lacking. An additional problem with such measurements for carbon nanofibers is the contribution of different sections that make up their structure and the number of parameters required to characterize them. The strength of SWCNTs depends only on their diameter[21] and that of multiwall carbon nanotubes on their diameter and wall thickness, both of which can usually be determined as a part of strength measurements. Even if we restrict the study to conical nanofibers, they will require the measurement of inner and outer wall thicknesses and cone angles, in addition to their diameter, to fully characterize their morphology.[8,10] Given the variety of morphologies that can be present in nanofiber samples, with various orientations of graphene sheets in them, the elastic properties may be quite different for each individual nanofiber. This means that attempts to measure only the elastic modulus of nanofibers without the corresponding morphology are of little value.

An attempt made in a recent study clearly illustrates the difficulties involved in determining the elastic modulus of conical carbon nanofibers.[22] Direct measurements of elastic properties were not attempted, but the investigators estimated a composite elastic modulus by assuming that the inner layer had a perfect graphitic stacked cone structure, while the structure of the outer layer was allowed to vary from perfectly graphitic multiwall nanotubes to turbostratic layers. Additionally, the elastic modulus of the inner layer was calculated assuming the modulus of a single graphene sheet, ignoring the much weaker forces between the sheets. Predictably, the composite elastic modulus from these calculations varied from 775 GPa for perfect graphitic sheets (which is close to the theoretical maximum of ~1 TPa) to 110 GPa for turbostratic outer layers. While useful as an exercise in attempting to solve a difficult problem, such an estimate cannot be treated as a reliable measure of VGCNF elastic properties.

As discussed above, an AFM-based bending test is best suited for measuring the elastic moduli of carbon nanofibers, but this needs to be combined with a method to determine the morphology of the individual nanofibers. In the bending tests nanotubes or nanofibers are suspended on a membrane,[11] on silicon substrates,[12,13] or on grooves etched on silicon wafer followed by deflection with an AFM probe.[14] While this approach allows for rapid determination of the modulus it does have several drawbacks. Polishing the membrane is not trivial and the weak adhesion of the nanomaterial on the membrane surface results in poor reproducibility. The method of fixing the fibers on silicon substrates avoids these issues.[13] Also, in these techniques the inner and outer diameters of the suspended nanomaterial are measured from the AFM image which convolutes the tip shape with the feature being imaged. Deconvolution of these images is not easy, and it introduces significant errors to the measurement. Additionally, the convolution of shapes by AFM means that these techniques do not allow the nanomaterials to be imaged at high resolution to determine their morphology.

Recently, an *in situ* measurement of the elastic modulus of MWCNTs was carried out inside a TEM using a hybrid nanorobotic manipulator.[23] In this technique a special manipulator was constructed and used interchangeably inside SEM and TEM holders. The nanotube sample was mounted on an AFM tip placed in the manipulator using electron beam-induced deposition inside a SEM. The nanotube was then deflected using a tungsten probe by placing the manipulator inside the TEM holder. The elastic modulus was obtained from the buckling of the nanotube and the morphology was determined from a high resolution TEM micrograph. The elastic modulus was determined to be in the range of ~1.23 TPa.

While the above approach is perhaps the best approach for elastic property measurements for single nanotubes and nanofibers, it requires specialized equipment that needs to be constructed. We have developed an accurate method combining readily available AFM, transmission electron microscopy (TEM) and focused ion beam (FIB) technology to determine the elastic properties of nanofibers and their morphology which eliminates the shortcomings of previous methods, but does not require any specialized equipment. We report the elastic modulus of individual VGCNFs determined using this method and demonstrate its use to study the dependence of elastic properties on the morphology of VGCNF. Pyrograf III carbon nanofibers obtained from Applied Science Inc. (Cedarville, Ohio) were well dispersed in ethanol using ultrasonication. A 2000 mesh copper grid was used as a template to suspend the nanofibers to measure their elastic properties and corresponding morphology. A droplet of the suspension was then deposited on the copper grid. The grid was carefully examined under an optical microscope to find nanofibers that lay across square gaps in the grid template. After identifying the desired nanofibers, the grid was mounted on a FEI Nova Nanolab FIB

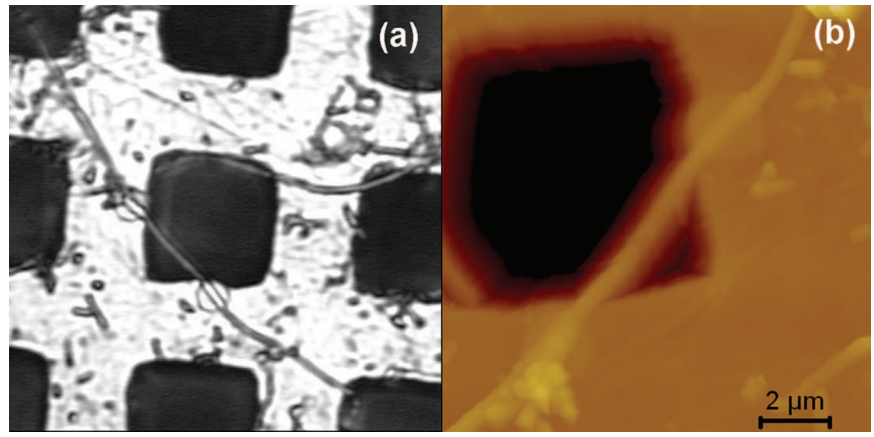

Figure 1. Suspended nanofiber fixed at both ends by platinum pads diagonally across the middle gap: (a) optical micrograph, and (b) corresponding AFM height image of the fixed nanofiber shown in panel a.

system, which was used to deposit 200 nm thick platinum pads on both ends of each nanofiber lying across a gap.[24] This ensured that the suspended portion of the nanofiber was securely attached to both ends of the gap as shown in Figure 1a.

A JEOL 300 KV LaB6 TEM was used to obtain high resolution TEM images of the suspended nanofiber. For each nanofiber considered, the average values of the inner diameter *d* and outer diameter *D* were obtained from several measurements taken at various points over the suspended length of the nanofiber. The TEM images were also used to determine the morphology of the nanofibers. In particular, for conical nanofibers the cone angle θ, the wall thickness *t*, and the thickness of the ordered inner layer and disordered outer layer were measured. The cone angle, outer diameter, and inner diameter are shown in Figure 2, and the ordered and disordered layers are shown in Figure 3.

The suspended length *L* (*i.e.*, the distance between supports) was recorded using the electron beam imaging mode in FIB. The grid was again examined under the optical microscope and the locations of nanofibers attached with platinum pads were identified. The grid was then carefully mounted on a Digital Instruments, multimode AFM with Nanoscope IIIa controller and imaged using the tapping-mode to locate the same suspended nanofiber (Figure 1b). A nanoscale three-point bend test was performed using the AFM probe to measure the elastic modulus of the suspended nanofiber.

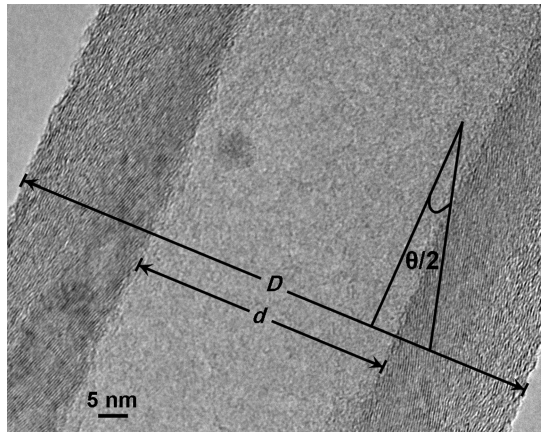

Figure 2. TEM micrograph showing the measured inner diameter (*d*), outer diameter (*D*), and the cone angle (θ) for a conical nanofiber.

For all nanofibers tested, the initial portion of the unloading curve did not coincide with the loading curve. This phenomenon is often observed when conducting bending tests with the AFM and is thought to be due to the adhesion of the AFM tip to the nanofiber during the retracting cycle.[25] Beyond this region, however, the loading and unloading curves were found to coincide as shown in Figure 4, indicating that the deformation of the nanofiber was elastic during the experiments. Since the aspect ratios (*i.e.*, ratios of *L* to *D*) for the nanofiber segments tested were between 10 and 20, beam theory is valid for this application and shear deformations can be neglected.

The elastic modulus *E* for each nanofiber was obtained from a linear fit of the loading force versus deflection curve beyond the contact point. The nanofibers were assumed to be prismatic beams of hollow circular cross-section. The values of the elastic modulus obtained from multiple bend tests for 17 different nanofibers are reported in Table 1. Post-test TEM micrographs indicated that the nanofibers remained intact after repeated three point bend tests and there was no indentation or damage made by the AFM probe during the deflection. For each individual fiber, at least six bend tests were performed and the *E* values, along with the standard deviation error, did not show significant variation as shown in Table 1. This provided further confirmation that the fibers remained intact and that the deflections of the nanofibers were within the elastic range for all samples. The consistency of the results for individual fibers also illustrates the repeatability of the experimental method.

The experimental technique developed here can be used to study the dependence of elastic modulus on morphology since the same fiber used in the AFM bend test

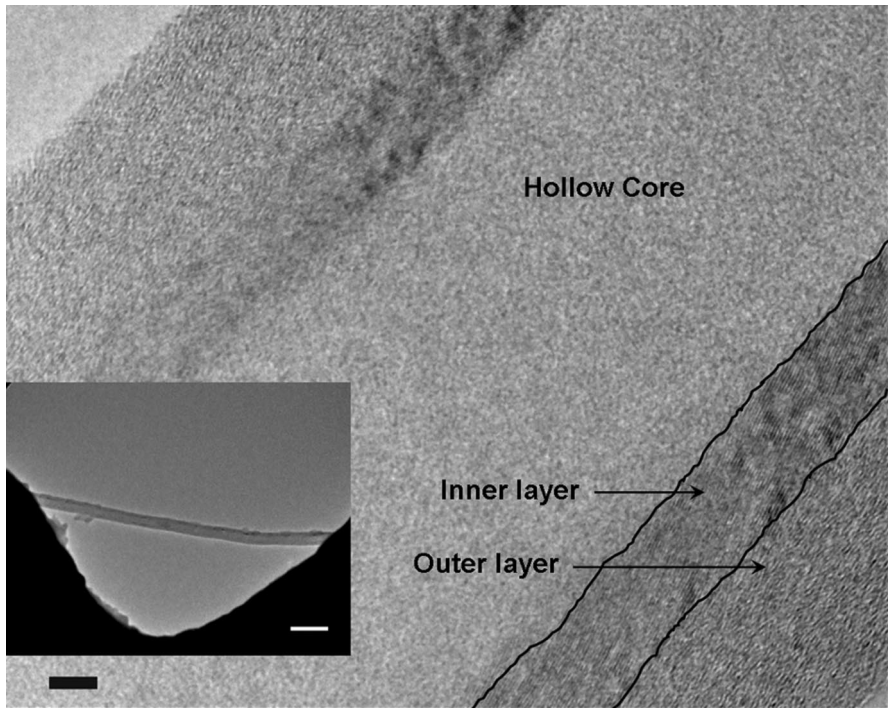

Figure 3. TEM micrograph showing the morphology of the same nanofiber shown in Figure 1. The disordered outer wall and ordered inner wall with conical graphene layers are clearly visible. The inset shows the low resolution TEM micrograph of the same nanofiber. The solid lines represent 5 nm in the figure and 500 nm in the inset.

can be studied using high resolution TEM imaging. For the nanofibers tested, the cone angles, thickness of the ordered inner layer and disordered outer layer were measured and are listed in Table 1. The high resolution images reduce the error in measuring the inner and outer diameters since these values are obtained directly, unlike other methods which use deconvoluted AFM images. As a result, the uncertainty in the measurements is no longer due to the instruments, but due to nonuniformities in the nanofibers themselves. The average variation, based on at least six measurements for each nanofiber, was found to be ± 3 nm, and this was used for all measured dimensions in Table 1.

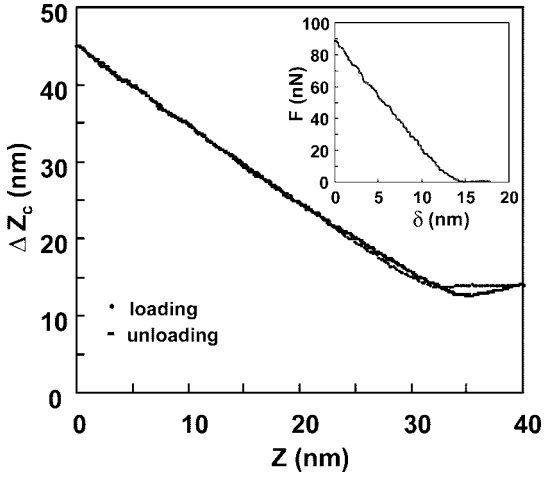

Figure 4. AFM cantilever deflection (ΔZ_c) plotted against the vertical coordinate of the piezo (Z) during the pushing−retracting cycle for the suspended nanofiber. The inset shows the force F plotted against the nanofiber deflection δ curve for the loading cycle.

A separate test was conducted to demonstrate the effectiveness of this method to determine any defects caused by the AFM tip to the nanofiber during the testing process, which was not feasible in the earlier AFM only methods. Two different nanofibers, one with a thicker outer layer and the other with a thinner one, were subjected to higher loading forces. The nanofiber with a thicker outer layer was found to crack at the point of contact when subjected to a loading force of 840 nN and still remain intact due to the support provided by the outer layer. For the case of the thinner outer layer, the nanofiber fractured at a loading force of 190 nN. The results from the two tests are shown in Figure 5.

For the conical nanofibers, the results from Table 1 suggest that the elastic modulus depends on various morphological parameters, such as the cone angle, thickness of the inner layer and the ratio of the outer layer to wall thickness. However, a closer examination shows that the most important parameter is the wall thickness t. Additionally, the data suggest that the relative fractions of the ordered inner layer and the disordered outer layer causes there to be two distinct property regimes for the elastic modulus. When the disordered outer layer is larger than the ordered inner layer, with $t_{out}/t > 0.5$, values of the elastic modulus can be much larger. For two fibers of the same thickness, such as for fibers no. 4 and no. 9 in Table 1, the value of E when $t_{out}/t > 0.5$ can be almost an order of magnitude greater than when $t_{out}/t < 0.5$.

TABLE 1. Measured Distance between Supports (*L*), Outer Diameter (*D*), Inner Diameter (*d*), Wall Thickness (*t*), Elastic Modulus (*E*), Cone Angles (θ), Inner Layer Thickness (t_{in}), Outer Layer Thickness (t_{out}) and Ratio of Outer Layer Thickness to Wall Thickness for Different Nanofibers[a]

fiber no.	*L* (μm)	*D* (nm)	*d* (nm)	*t* (nm)	*E* (GPa)	θ (deg)	t_{in} (nm)	t_{out} (nm)	t_{out}/t
1	4.8	185 ± 3	75 ± 3	55 ± 3	81 ± 6	24	20 ± 3	35 ± 3	0.64
2	7.1	295 ± 3	152 ± 3	70 ± 3	37 ± 3	44	35 ± 3	35 ± 3	0.50
3	4.9	170 ± 3	73 ± 3	50 ± 3	93 ± 8	40	25 ± 3	25 ± 3	0.50
4	7.3	174 ± 3	92 ± 3	45 ± 3	160 ± 7	41	20 ± 3	25 ± 3	0.56
5	6.2	325 ± 3	205 ± 3	60 ± 3	6 ± 0.2	58	50 ± 3	10 ± 3	0.17
6	8.3	227 ± 3	145 ± 3	40 ± 3	95 ± 9	19	20 ± 3	20 ± 3	0.50
7	4.3	195 ± 3	67 ± 3	65 ± 3	23 ± 2	39	50 ± 3	15 ± 3	0.23
8	9.2	115 ± 3	52 ± 3	30 ± 3	207 ± 1	20	10 ± 3	20 ± 3	0.67
9	5.9	260 ± 3	170 ± 3	45 ± 3	20 ± 0.4	30	35 ± 3	10 ± 3	0.22
10	5.1	198 ± 3	76 ± 3	61 ± 3	60 ± 4	40	22 ± 3	39 ± 3	0.64
11	8.3	230 ± 3	80 ± 3	75 ± 3	37 ± 0.6	41	23 ± 3	52 ± 3	0.69
12	5.4	184 ± 3	124 ± 3	30 ± 3	69 ± 5	40	20 ± 3	10 ± 3	0.33
13	3.7	176 ± 3	84 ± 3	46 ± 3	105 ± 9	40	22 ± 3	24 ± 3	0.52
14	2.5	153 ± 3	50 ± 3	52 ± 3	55 ± 4	30	30 ± 3	22 ± 3	0.42
15	5.9	450 ± 3	190 ± 3	130 ± 3	32 ± 0.7				
16	8.2	470 ± 3	260 ± 3	105 ± 3	13 ± 0.6				
17	8.3	315 ± 3	65 ± 3	125 ± 3	25 ± 0.6				

[a]Here θ, t_{in} and t_{out} were not measured for the last three nanofibers due to large values of *t* which limited the resolution.

The above trends are shown in Figure 6a. The values of *E* for $t_{out}/t \geq 0.5$ show an inverse relationship with *t*, decreasing rapidly from a value as high as 207 GPa as the wall thickness increases. However, the value of *E* seems to bottom out at ~25 GPa and remains at that value even for very thick fibers. This suggests, counterintuitively, that thinner fibers have greater strength than the thicker ones. There are fewer nanofibers in our sample with $t_{out}/t < 0.5$, but they show a similar trend although it is somewhat less pronounced.

The significant decrease in *E* when the outer-wall thickness is less than that of the inner wall strongly suggests that it is the outer wall that contributes primarily to the strength of conical nanofibers. When the relative thickness of the outer wall becomes very small, such as a t_{out}/t of 0.17 for fiber no. 5 in Table 1, the value of *E* can drop as low as 6 GPa. This suggests that it may be more appropriate to calculate *E* assuming that the load is entirely taken up by the outer wall in the three-point bending test. Figure 6b shows the dependence of the recalculated *E* on the wall thickness and it is clear that the $t_{out}/t < 0.5$ data and the $t_{out}/t \geq 0.5$ data now match more closely.

The dominance of the outer wall in contributing to the strength of conical nanofibers has been suggested before.[10] This is due to the weakness of the interactions between the helical graphene planes in the inner layer which cannot provide much load-bearing support. However, the decrease in *E* with the wall thickness is surprising as increasing thickness of the outer layer can be expected to stiffen the nanofibers. The most likely reason for this is the increasing imperfection of the outer wall as more layers are added to it, as can be seen in Figure 3. These additional layers may not be contributing to the strength of the nanofiber, resulting in lowered values for *E* when it is calculated assuming that the

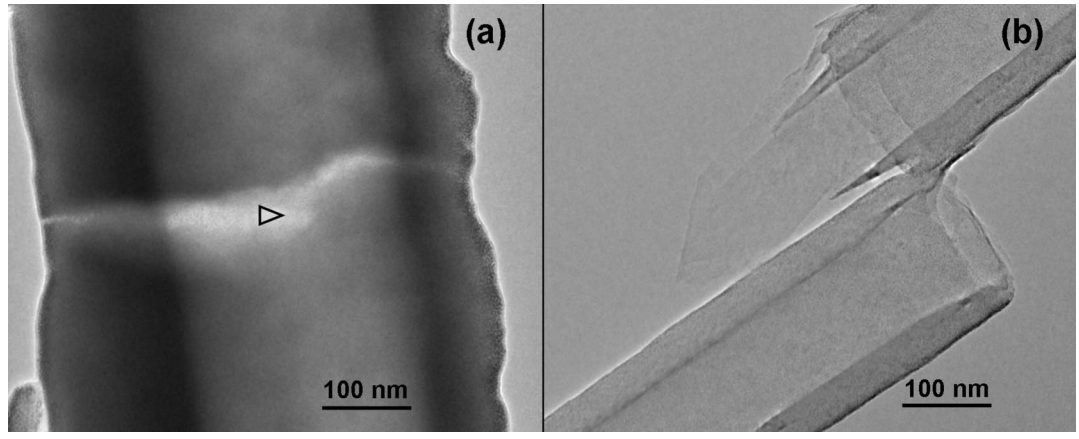

Figure 5. TEM micrographs of nanofibers tested using large forces: (a) nanofiber with thick outer layer showing a crack in the middle, and (b) nanofiber with thin outer layer following fracture. The triangle in panel a represents the point of contact of the AFM tip.

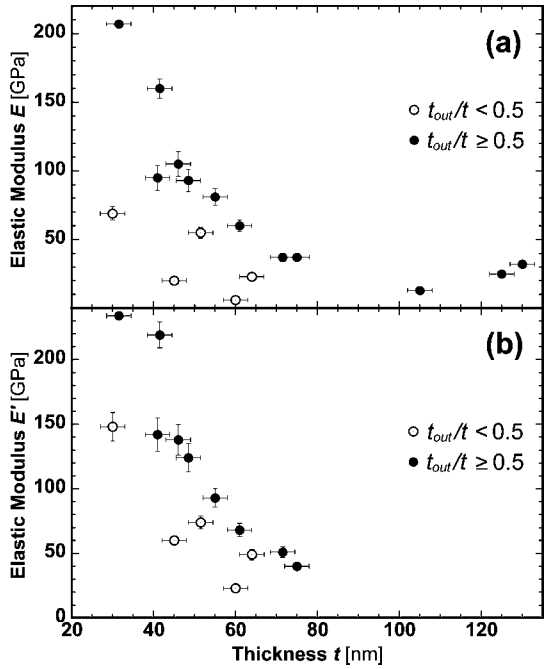

Figure 6. Plots of the elastic moduli of nanofibers for different wall thicknesses: (a) when the load is assumed to be borne by both inner and outer walls, and (b) the recalculated elastic modulus E' assuming that the load is borne only by the outer wall. In both cases data corresponding to $t_{out}/t < 0.5$ and $t_{out}/t \geq 0.5$ are shown. The fibers with $t > 80$ nm are not shown in panel b as their t_{out} could not be measured.

entire wall is load bearing. This also agrees with anecdotal evidence that thinner grade nanofibers are preferred for most applications, such as the PR-24 grade Pyrograf III nanofibers produced by ASI. If this is valid then the correct value of E for the load bearing parts of the nanofiber will be much larger than that reported in Table 1, and may approach those reported for MWCNTs.

Finally, the data in Figure 6a suggests that for thick fibers with $t > 80$ nm, the trend changes and the elastic moduli become largely independent of the thickness. This seems to be a distinct region with the modulus having a low value of ~25 GPa, but larger than the low values reached by the fibers with $t_{out}/t < 0.5$. This most likely represents the transition from nanoscale properties to bulk behavior, with nanofiber properties becoming closer to those of low grade carbon fiber rather than the high values associated with nanotubes. This is probably a reflection of the fact that at thicknesses of $t > 80$ nm the nanofiber now mostly consists of turbostratic graphene layers.

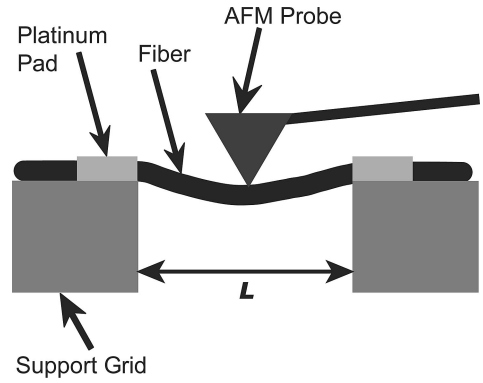

Figure 7. Schematic of the three-point bend test of the single nanofiber fixed on the grid by platinum pads using the AFM tip. L is the suspended length.

In summary, we have developed a method to reproducibly measure the elastic properties and morphology of individual carbon nanofibers. The inner and outer diameters of the suspended nanofibers were measured with greater accuracy compared to most previous methods. The morphology of the nanofiber and associated properties, such as cone angles, thickness of the inner layer, and thickness of the outer layer were also measured. The nanoindentation technique did not damage the nanofibers during measurements, unless an extremely high load was employed. The values of E also showed two distinct trends, with higher values when the outer wall thickness is larger than that of the inner wall. Additionally, the values decreased with the overall wall thickness, suggesting that the added layers were not load bearing. These results suggest that the more ordered layers of the outer wall, closest to the inner wall, are mostly responsible for the nanofiber strength. For large nanofiber wall thicknesses of $t > 80$ nm the elastic modulus becomes independent of the thickness with a value of ~25 GPa. The results also demonstrate that this technique combining TEM, AFM, and FIB can be a standardized one for the detailed study of the mechanical properties of nanofibers and their relationship to morphology. As expected, the measured values of the elastic modulus by this method for conical nanofibers did not match those for SWCNTs and MWCNTs, but they could be as high as 200 GPa or larger.

METHODS

The grid with the suspended nanofiber was mounted on the AFM and imaged using the tapping-mode to locate the same nanofiber. The nanoscale three-point bend test was performed using an AFM probe as shown in the schematic in Figure 7. A maximum load of 90 nN was applied with a loading rate of 1 μm/s at the midspan. During the pushing−retracting cycle, the cantilever deflection (ΔZ_c) versus the vertical coordinate of the piezo (Z) was recorded. AFM probes with cantilevers of spring constant of 5 N/m (datum supplied by the manufacturer) were used in these experiments.

The values for applied force, F, and midspan deflection of the nanofiber δ, were obtained from the AFM force curves. A description of the method can be found in other studies.[13,26] Briefly, the applied force was calculated from the deflection of the cantilever by the relation $F = k\Delta Z_c$, where k is the spring constant of the AFM cantilever. Since the vertical displacement of the piezo is the sum of the deflections of the suspended

nanofiber and the cantilever, the deflection of the nanofiber was obtained by subtracting the displacement of the cantilever from the total displacement of the piezo by the relation, $\delta = \Delta Z - \Delta Z_c$. Here ΔZ is the offset of the displacement of the piezo from the contact point of the AFM tip with the suspended nanofiber. For all of our experiments, δ was found to be linear with F. This is consistent with beam theory which states that for a fixed-end beam, the relationship between a concentrated force F, applied at the midspan and the deflection δ of the point of application of the force is given by the equation[27]

$$F = \frac{192EI}{L^3}\delta \quad (1)$$

Here E, I, and L are the elastic modulus, second area moment of the cross-section, and the beam span, respectively.

Acknowledgment. The authors acknowledge Drs. Kai Sun and Haiping Sun of EMAL at the University of Michigan for their assistance with TEM and FIB analyses. This study was financially supported by Army Research Office Grants DAAD19-03-1-0012 and W911NF-05-1-0542.

REFERENCES AND NOTES

1. Tibbetts, G. G.; Gorkiewics, D. W.; Alig, R. L. A New Reactor for Growing Carbon Fibers from Liquid and Vapor-Phase Hydrocarbons. *Carbon* **1993**, *31*, 809–814.
2. Tibbetts, G. G.; Bernardo, C. A.; Gorkiewics, D. W.; Alig, R. L. Role of Sulfur in the Production of Carbon Fibers in the Vapor Phase. *Carbon* **1994**, *32*, 569–576.
3. Tibbetts, G. G.; Lake, M. L.; Strong, K. L.; Rice, B. P. A Review of the Fabrication and Properties of Vapor Grown Carbon Nanofiber/Polymer Composites. *Compos. Sci. Technol.* **2007**, *67*, 1709–1718.
4. Xu, L. R.; Bhamidipati, V.; Zhong, W. H.; Li, J.; Lukehart, C. M. Mechanical Property Characteriztion of a Polymeric Nanocomposite Reinforced by Graphitic Nanofibers with Reactive Linkers. *J. Comput. Mater.* **2004**, *38*, 1563–1581.
5. Lazano, K.; Yang, S.; Jones, J. E. Nanofiber Toughened Polyethylene Composites. *Carbon* **2004**, *42*, 2329–2331.
6. Choi, Y. K.; Sugimoto, K. I.; Song, S. M.; Endo, M. Mechanical and Thermal Properties of Vapor-grown Carbon Nanofiber and Polycarbonate Composite Sheets. Y. *Mater. Lett.* **2005**, *59*, 3514–3520.
7. Endo, M.; Kim, Y. A.; Hayashi, T.; Fukai, Y.; Oshida, K.; Yanagisawa, T.; Higaki, S.; Dresselhaus, M. S. Structural Characterization of Cup-Stacked-type Nanofibers with an Entirely Hollow Core. *Appl. Phy. Lett.* **2002**, *80*, 1267–1269.
8. Collins, S.; Brydson, R.; Rand, B. Structural Analysis of Carbon Nanofibers Grown by the Floating Catalyst Method. *Carbon* **2002**, *40*, 1089–1100.
9. Eksioglu, B.; Nadarajah, A. Structural Analysis of Conical Carbon Nanofibers. *Carbon* **2006**, *44*, 360–373.
10. Lawrence, J. G.; Berhan, L. M.; Nadarajah, A.; Structural Transformation of Vapor Grown Carbon Nanofibers Studied by HRTEM. *J. Nanopart. Res.*, published online December, 18, 2007,, DOI: 10.1007/s11051-007-9341-4.
11. Salvetat, J.-P.; Briggs, G. A. D.; Bonard, J.-M.; Bacsa, R. R.; Kulik, A. J.; Stockli, T.; Burnham, N. A.; Forro, L. Elastic and Sheer Moduli of Single-Walled Carbon Nanotube Ropes. *Phys. Rev. Lett.* **1999**, *82*, 944–947.
12. Walters, D. A.; Ericson, L. M.; Casavant, M. J.; Liu, J.; Colbert, D. T.; Smith, K. A.; Smalley, R. E. Elastic Strain of Freely Suspended Single-wall Carbon Nanotube Ropes. *Appl. Phys. Lett.* **1999**, *74*, 3803–3805.
13. Kim, G.-T.; Gu, G.; Waizmann, U.; Roth, S. Simple Method to Prepare Individual Suspended Nanofibers. *Appl. Phys. Lett.* **2002**, *80*, 1815–1817.
14. Tan, E. P. S.; Lim, C. T. Physical Properties of Single Polymeric Nanofiber. *Appl. Phys. Lett.* **2004**, *84*, 1603–1605.
15. Demczyk, B. G.; Wang, Y. M.; Cumings, J.; Hetman, M.; Han, W.; Zettl, A.; Ritchie, R. O. Direct Mechanical Measurement of the Tensile Strength and Elastic Modulus of Multiwalled Carbon Nanotubes. *Materials Sci. Eng. A.* **2002**, *334*, 173–178.
16. Krishnan, A.; Dujardin, E.; Ebbesen, T. W.; Yianilos, P. N.; Treacy, M. M. J. Young's Modulus of Single-walled Nanotubes. *Phys. Rev. B.* **1998**, *58*, 14013–14019.
17. Tan, E. P. S.; Lim, C. T. Novel Approach to Tensile Testing of Micro- and Nanoscale Fibers. *Rev. Sci. Instrum.* **2004**, *75*, 2581–2585.
18. Tan, E. P. S.; Goh, C. N.; Sow, C. H.; Lim, C. T. Tensile Test of a Single Nanofiber Using an Atomic Force Microscope Tip. *Appl. Phys. Lett.* **2005**, *86*, 073115-1–073115-3.
19. Yu, M-F.; Lourie, O.; Dyer, M. J.; Moloni, K.; Kelly, T. F.; Ruoff, R. S. Strength and Breaking Mechanism of Multiwalled Carbon Nanotubes Under Tensile Load. *Science* **2000**, *287*, 637–640.
20. Wei, C.; Srivastava, D. Nanomechanics of Carbon Nanofibers: Structural and Elastic Properties. *Appl. Phys. Lett.* **2004**, *85*, 2208–2210.
21. Natsuki, T.; Tantrakarn, K.; Endo, M. Effects of Carbon Nanotube Structures on Mechanical Properties. *Appl. Phys. A: Mater. Sci. Process.* **2004**, *79*, 117–124.
22. Uchida, T.; Anderson, D. P.; Minus, M. L.; Kumar, S. Morphology and Modulus of Vapor Grown Carbon Nanofibers. *J. Mater. Sci.* **2006**, *41*, 5851–5856.
23. Nakajima, M.; Arai, R.; Fukuda, T. *In Situ* Measurement of Young's Modulus of Carbon Nanotubes Inside a TEM Through A Hybrid Nanorobotic Manipulation System. *IEEE Trans. Nanotechnol.* **2006**, *5*, 243–248.
24. Dovidenko, K.; Rullan, J.; Moore, R.; Dunn, K. A.; Geer, R. E.; Heuchling, F. FIB-Assisted Pt Deposition for Carbon Nanotube Integration and 3-D Nanoengineering. *Mater. Res. Soc. Symp. Proc.* **2003**, *739*, 193–198.
25. Sanchez, M. S.; Mateo, J. M.; Colomer, F. J. R.; Ribelles, J. L. G. Nanoindentation and Tapping mode AFM Study of Phase Separation in Poly(ethyl acrylate-*co*-hydroxyethy methacrylate) Copolymer Networks. *Eur. Polym. J.* **2006**, *42*, 1378–1383.
26. Tombler, T. W.; Zhou, C.; Alexseyev, L.; Kong, J.; Dal, H.; Liu, L.; Jayanthi, C. S.; Tang, M.; Wu, S.-Y. Reversible Electromechanical Characteristics of Carbon Nanotubes under Local-Probe Manipulation. *Nature* **2000**, *405*, 769–772.
27. Gere, J. M.; Timoshenko, S. P. *Mechanics of Materials*; PWS Publishing Company: Boston, MA, 1990.